Vertical Drop Testing and Simulation of Anthropomorphic Test Devices

Michael A. Polanco, Justin D. Littell
ATK Space Systems
Hampton, Virginia 23681
michael.a.polanco@nasa.gov
justin.d.littell@nasa.gov

Abstract

A series of 14 vertical impact tests were conducted using Hybrid III 50th Percentile and Hybrid II 50th Percentile Anthropomorphic Test Devices (ATDs) at NASA Langley Research Center. The purpose of conducting these tests was threefold: to compare and contrast the impact responses of Hybrid II and Hybrid III ATDs under two different loading conditions, to compare the impact responses of the Hybrid III configured with a nominal curved lumbar spine to that of a Hybrid III configured with a straight lumbar spine, and to generate data for comparison with predicted responses from two commercially available ATD finite element models. The two loading conditions examined were a high magnitude, short duration acceleration pulse, and a low magnitude, long duration acceleration pulse, each created by using different paper honeycomb blocks as pulse shape generators in the drop tower. The test results show that the Hybrid III results differ from the Hybrid II results more for the high magnitude, short duration pulse case. The comparison of the lumbar loads for each ATD configuration show drastic differences in the loads seen in the spine. The analytical results show major differences between the responses of the two finite element models. A detailed discussion of possible sources of the discrepancies between the two analytical models is also provided.

Introduction

The evolution of occupant injury protection and prevention has led to the development of Anthropomorphic Test Devices (ATDs, also commonly known as crash test dummies) by researchers over the past 60 years. These ATDs have been used in countless ways leading to advancements in occupant protection systems for both automobiles and aircraft. Their history has been thoroughly documented [1], however, a brief summary is provided here as reference.

The first crash test dummy, Sierra Sam, was developed in 1949 by the U.S. Air Force for use in ejection seat testing. However, it lacked much of the bio-fidelity needed for frontal impact loading conditions to accurately assess injury in automotive crashes. Developments from this original dummy lead to the first Hybrid II series of ATDs, which were the first set of standardized dummies used in the automotive industry. The original Hybrid II family of ATDs was developed in 1972 by General Motors for assessment of restraint systems.

This dummy proved to be a valuable tool in the evaluation of restraint systems and was recognized in official guidelines such as the Federal Motor Vehicle Standard 208 [2]. The Hybrid II remained the standard in automotive testing until the Hybrid III family of ATDs was introduced in 1987. The Hybrid III addressed deficiencies of the Hybrid II, mainly in the area of the neck performance and provided improved bio-fidelity. The Hybrid III ATD also used a curved spine which better represented the occupant in a sitting position, as opposed to the original Hybrid II straight spine. The Hybrid III is still the standard in automotive crash testing; however, newer specialized ATDs are in development, which look to improve on the Hybrid III standard.

The aerospace industry relies heavily on the developments of automotive dummies and injury criteria originally developed for automotive use. However, the aerospace industry must address injuries associated with vertical loading conditions (i.e. an aircraft crash scenario) individually or in conjunction with horizontal loading conditions, which are largely ignored in the automotive world. Thus, the aerospace industry must develop its own specialized guidelines. One example is from the Federal Aviation Administration (FAA). Federal Aviation Regulation (FAR) 27.562 Subpart C "Emergency Landing Conditions" [3] has established

guidelines on occupant injury, which establishes a 1,500 lb limit on vertical lumbar loading from a "…170 lb [50th percentile] ATD". However, the choice of the ATD is not specified. It is common for researchers in the aerospace fields to use a Hybrid III ATD modified to include the straight lumbar spine originally used on the Hybrid II ATD, as documented in [4]. The straight spine is used in the aerospace industry because it is commonly believed to better replicate the seated position of the occupant than a Hybrid III ATD with a curved spine. The differences between the Hybrid II, Hybrid III with curved spine and Hybrid III with straight spine are not well understood.

At NASA Langley Research Center (LaRC), researchers have conducted full-scale crash tests and simulations of aircraft involving ATD occupants [5-9] using variations of the Hybrid III and Hybrid II. Elsewhere, researchers have used the various ATDs in aircraft loading conditions to establish limits for lumbar loading with regard to military seats [10], to evaluate seat performance [11], and to evaluate injury due to ejection seat loading [12]. Researchers at Wright Patterson Air Force Base commonly test dummies in their Vertical Decelerator Tower [13-14] which simulates ejection seat loading and evaluates the effect of variables such as helmets, and seating posture. NASA is also examining the feasibility of including ATDs in the Orion spacecraft [15] testing and simulations. The performance and accuracy of these ATDs are critical when evaluating probable risks of injury for crew under an aircraft crash or spacecraft landing.

To address these concerns, a research program was undertaken at NASA LaRC to examine vertical loading responses using three common configurations of ATDs. A Hybrid III with a straight spine, Hybrid III with a curved spine and a Hybrid II ATD were tested under vertical loading conditions to evaluate their performance and to generate data for correlation with predictions from two occupant simulation models. Along with the test series, an evaluation of two commercially available ATD Finite Element Models developed by Livermore Software Technology Company (LSTC) and First Technology Safety Solutions (FTSS) is presented.

Test Setup

All tests were conducted using a vertical drop tower at NASA LaRC. For each test configuration, the ATD sat on a rigid aluminum seat platform which was connected directly to the drop tower rails. The desired input pulse was generated by impacting the platform against layers of either weak paper honeycomb (nominal crush strength of 30 psi) or strong paper honeycomb (nominal crush strength of 50 psi). The average impact velocity was 17.3 ft/sec for tests conducted with the strong paper honeycomb and 16.6 ft/sec for tests conducted with the weak paper honeycomb. Figure 1 shows the test setup.
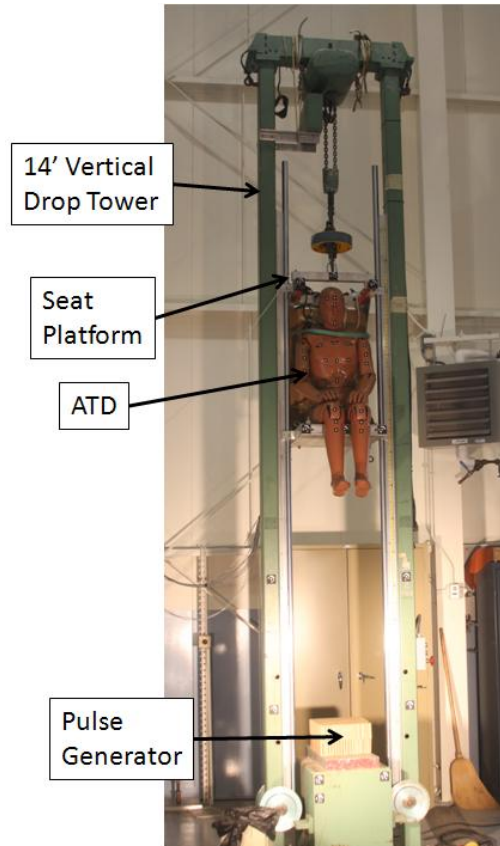

Figure 1 – Drop tower setup

During the test series, each ATD was instrumented with six accelerometers; two in the head, chest and pelvis measuring vertical (Z) and forward (X) accelerations, and a lumbar load cell, measuring vertical lumbar loads only. Lateral (Y) responses were assumed to be minor; therefore, no data was collected in the lateral direction. The platform was instrumented with two accelerometers measuring vertical (Z) acceleration. Data was sampled at 10 kHz and collected on a National Instruments NI-DAQ data acquisition system using LabView software.

Targets for three-dimensional photogrammetry were also placed on each ATD at specific locations to compare position measurements pre- and post-test, along with transient motion that occurred during the impact. Among the entire set, targets were placed at

both the head and chest CG locations. Other targets were placed to measure angular and relative motion between various components of the ATD, while some were placed and used for positioning in computer model development. Targets were also placed on the platform for the examination of flexure during the impact. Care was taken to place the targets in similar spots between the different ATD configurations; however, in one specific instance, the difference between the Hybrid III and the Hybrid II arm attachment and shoulder joints necessitated the placement of the targets in slightly different locations.

Each test was filmed with two high speed cameras at 1,000 frames per second (fps). All photogrammetry, high speed video, and acceleration data were time synchronized with an IRIG-B master clock. There were no restraints as part of the test setup so the ATD was free to move throughout the impact. Safety straps were loosely placed around the neck and waist to restrain the ATD within the platform. The final test setup is shown in Figure 2 with the straps, photogrammetry targets, and coordinate system highlighted.
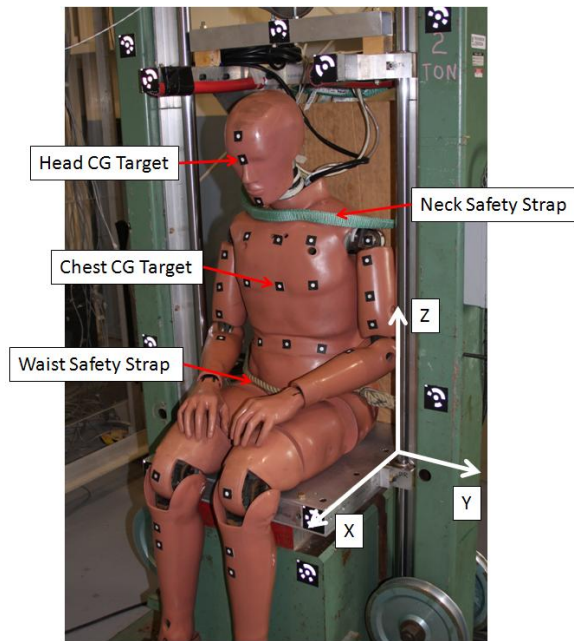

Figure 2 – Test setup

In total, 14 tests were completed. Multiple repeated tests were conducted for each ATD configuration to ensure consistency and repeatability of the data. The configuration of each test both included the specific ATD along with the honeycomb type. Thus, there were a total of six test configurations. Table 1 shows the test matrix, which lists both the repeated test numbers along with each test configuration. Tests 1-6 were preliminary tests conducted solely for the calibration of instrumentation and as a quality check of test methods, and are, therefore, not reported here. Note that data was lost from test 17 and, therefore cannot be reported.

Table 1 – Test Matrix

Test #	ATD	Spine	Pulse
7-9	HIII	Straight	Strong
10-12	HIII	Straight	Weak
13-14	HII	Straight	Strong
15-16	HII	Straight	Weak
18-19	HIII	Curved	Strong
20-21	HIII	Curved	Weak
HIII – Hybrid III			
HII – Hybrid II			

Test Results

The strong and weak paper honeycomb input pulses as measured on the platform are shown in Figure 3. The pulses are filtered with a 4-pole low pass Butterworth filter, with a cut off frequency of 1000 Hz.
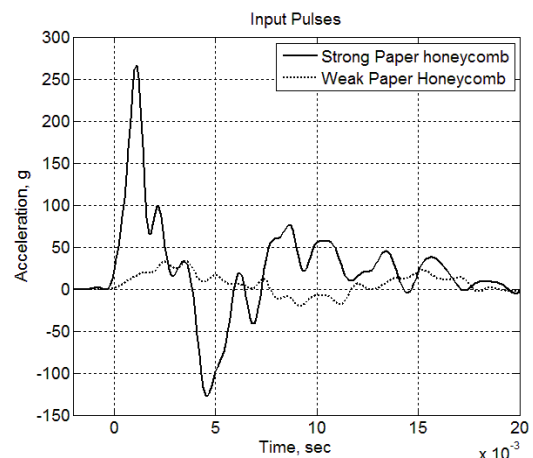

Figure 3 – Seat platform acceleration

The average peak acceleration from the tests with the strong paper honeycomb was 258 g, with an average pulse duration of 50 ms. The average peak acceleration from the tests with the weak paper honeycomb was 32 g, with an average pulse duration of 100 ms.

Representative lumbar loads are shown in Figure 4 for impacts onto strong paper honeycomb. The plot shows three curves with corresponding legend. The three curves are the Hybrid III with straight spine (Hybrid III, Straight), Hybrid II (Hybrid II, Straight) and Hybrid III with curved spine (Hybrid III, Curved). All ATD response data was filtered in accordance with SAE J211 CFC 600 [16].
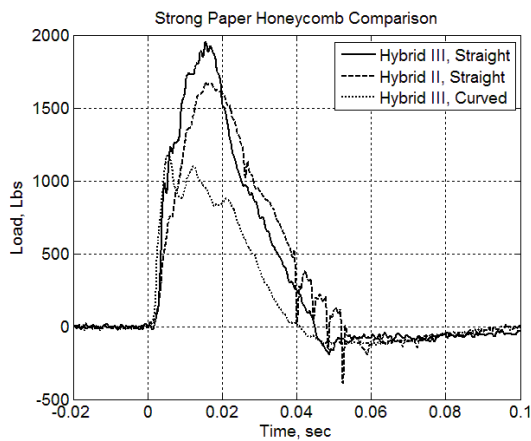
Figure 4 – Lumbar loads for strong paper honeycomb.

Note that if the lumbar load limit of 1,500 lbs. specified in FAR 27.562 is used, the ATD's which included the straight spines exceed this limit, while the ATD with the curved spine does not, indicating that the spinal configuration greatly affects the results. The results are significant because in all three tests the ATD weighed approximately the same at 170 lbs, and was positioned to within 1-in. for each test configuration (discussed later). The only difference was the lumbar spine. The Hybrid III with straight spine has a maximum load of 1,991 lbs, while the Hybrid II peak load is 1,755 lbs. The Hybrid III with curved spine sees the lowest load at 1,255 lbs.
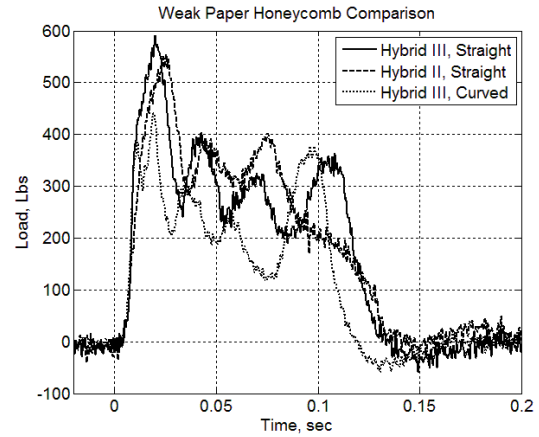

Figure 5 – Lumbar loads for weak paper honeycomb.

The lumbar load was also plotted for the weak paper honeycomb impact conditions, and is shown in Figure 5. The impacts onto weak paper honeycomb show considerably less load, and the peak values of load for the different ATD configurations showed less variation. The four individual peaks seen in each response time history are from the ATD crushing each individual layer of honeycomb. The Hybrid III with straight spine has the maximum load of 591 lbs, the Hybrid II peak load being 554 lbs. Finally, the Hybrid III with curved spine sees the lowest load at 450 lbs.

The trends in both impact cases provide some interesting insights. First, the loads in the curved spine are lower than loads in the straight spine. There are two possible reasons for this trend. The first is the orientation of the load cell for the curved spine configuration. The load cell in the curved spine configuration is oriented at a 22 deg angle from the vertical, while the straight load cell is oriented along the vertical axis. The spine itself is a column approximately 6 to 8 in. long and 3 in. in diameter. Another possibility is that the curved lumbar spine fundamentally creates a different load path through the ATD. The differences in spinal configuration are shown in Figure 6. Regardless of the reason, care must be taken in choosing a suitable spine.
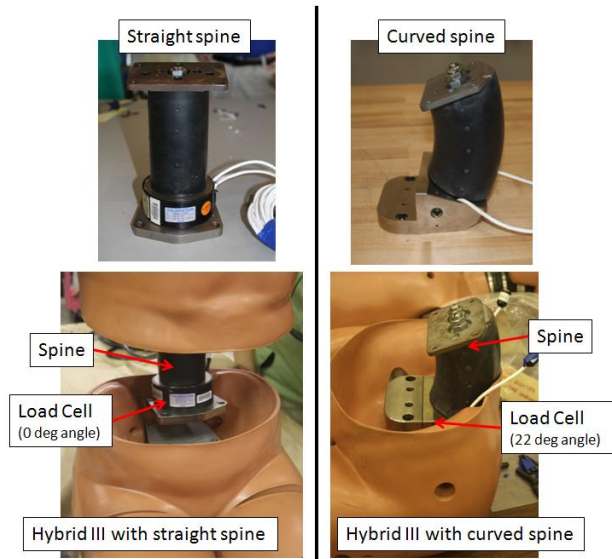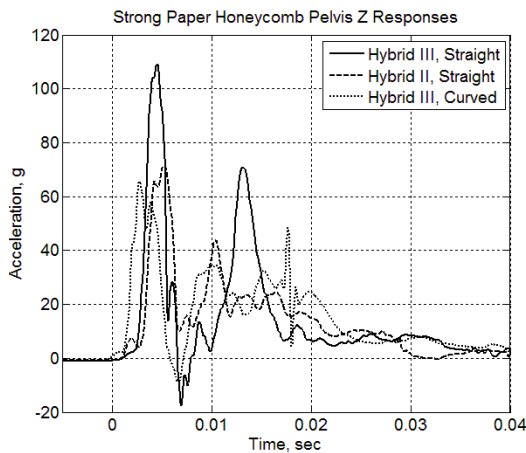
Figure 6 – Straight and curved lumbar spine

Next, representative acceleration time history curves for the head, chest, and pelvis of the Hybrid III with straight spine, Hybrid II and Hybrid III with curved spine were examined for the strong and weak paper honeycomb impacts. Figures 7 through 9 show the time history results from the vertical (z) direction.

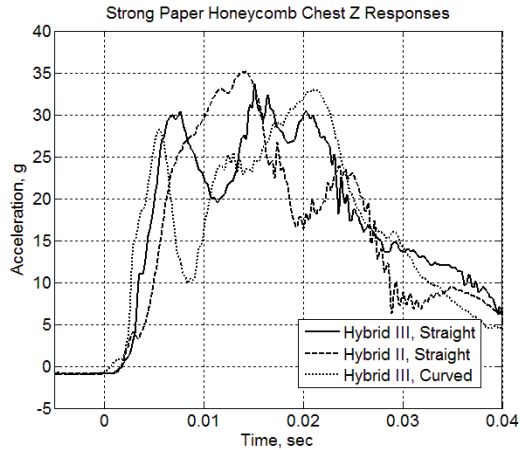(a) Strong paper honeycomb pelvis accelerations
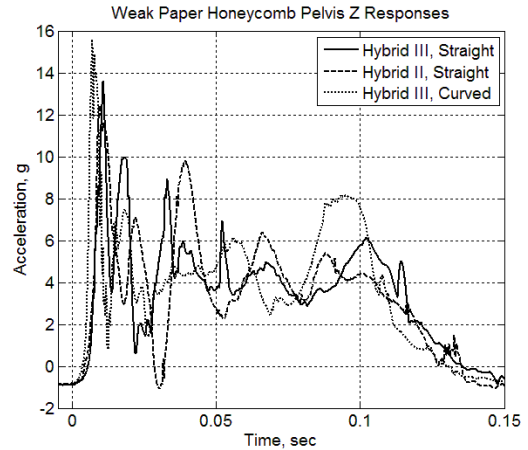
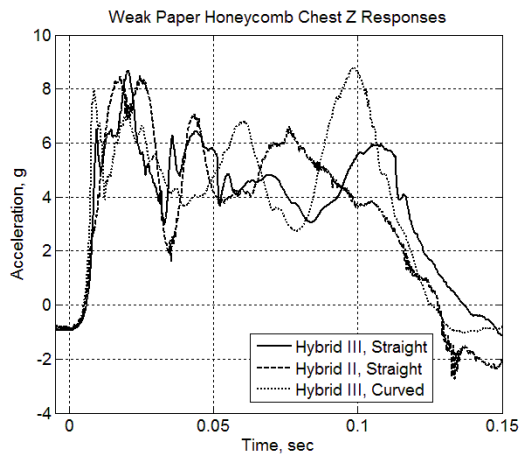

(b) Weak paper honeycomb pelvis accelerations

Figure 7 - Pelvis accelerations

Figure 7 shows the vertical pelvic accelerations for the three ATD configurations. With the exception of the Hybrid III with straight spine impacting strong paper honeycomb, all curves tend to be in good agreement. Note that in Figure 7(a), the width of the pulse is approximately 5 ms, while the width of the pulse for the weak paper honeycomb is approximately 100 ms. The shapes of the curves for the strong paper honeycomb accelerations show an initial peak at approximately 5 ms, followed by a decrease at approximately 7 ms. A second longer duration peak starts to occur around 10 ms. The double peaks in the response occur during sequential crushing of honeycomb layers. The peak values for each condition can be found in Tables 2 and 3.

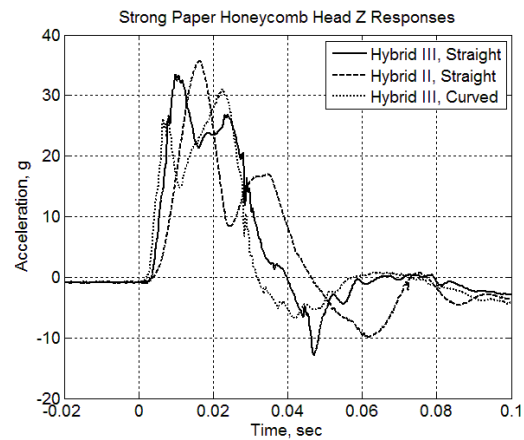(a) Strong paper honeycomb chest accelerations
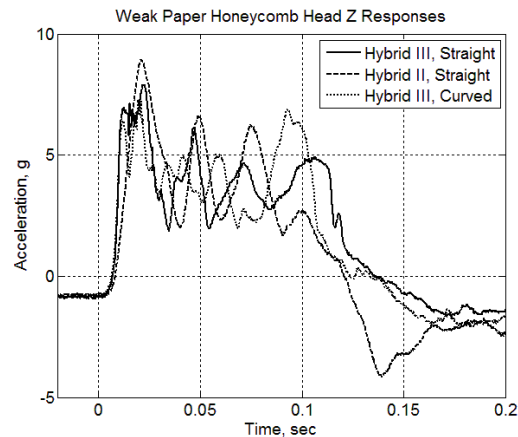

(b) Weak paper honeycomb chest accelerations

Figure 8 - Chest accelerations

Figure 8 shows the vertical chest accelerations for the three ATD configurations. All curves appear to exhibit similar trends. For both the strong and weak paper honeycomb, the pulse width for the chest was much longer than the pulse width for the pelvis, which is an indication that the internal response of the ATD shapes the measured pulse. The approximate width of the pulse for the strong paper honeycomb is approximately 40 ms while the width of the pulse for the weak paper honeycomb is approximately 120 ms. Generally, the acceleration magnitudes are lower in the chest than in the pelvis because of energy attenuation within the pelvis. Also note that there are four individual spikes in the weak paper honeycomb results. As previously seen with the lumbar load time histories, these peaks are a result of sequential crushing of the honeycomb layers.

Finally, vertical acceleration responses were plotted for the head. Figure 9(a) shows the strong paper honeycomb pulse while Figure 9(b) shows the weak paper honeycomb pulse. As with the chest accelerations, the trends between the three configurations match for both the strong and weak paper honeycomb cases. The pulse widths for the head are similar to the pulse widths of the chest for both cases. These results indicate that the loading shape changes between the pelvis and chest, but stays relatively the same between the chest and the head. Tables 2 and 3 summarize the results and list the averaged values measured in each ATD location, for each configuration. Table 2 lists the results from the strong paper honeycomb tests.

(a) Strong paper honeycomb head accelerations

(b) Weak paper honeycomb head accelerations

Figure 9 - Head Accelerations

Table 2 – Strong Paper Honeycomb Results

Location (direction)	HIII, S	HII	HIII, C
Lumbar Load (lb)	1991	1755	1255
Pelvis (Z) (g)	115	74.6	79.6
Pelvis (X) (g)	88.6	53.7	78.7
Chest (Z) (g)	33.4	36.6	32.5
Chest (X) (g)	17.6	5.5	20.2
Head (Z) (g)	35.5	36.4	30.7
Head (X) (g)	-7.9	-10.0	-10.0
HIII, S – Hybrid III, Straight Spine			
HII – Hybrid II			
HIII, C – Hybrid III, Curved spine			

The results in Table 2 show that aside from the lumbar pelvic region, the acceleration results are in good agreement. Possible discrepancies in the lumbar loads were previously discussed; however, the possible discrepancies in the pelvis accelerations may be due to a magnification factor. In a magnification factor, a tiny positional change leads to large differences in ATD response. Table 3 lists the results for the weak paper honeycomb tests.

Table 3 – Weak Paper Honeycomb Results

Location (direction)	HIII, S	HII	HIII, C
Lumbar Load (lb)	579	562	449
Pelvis (Z) (g)	14.5	13.3	13.2
Pelvis (X) (g)	11.6	7.3	13.5
Chest (Z) (g)	8.5	8.9	8.7
Chest (X) (g)	3.5	5.0	7.0
Head (Z) (g)	8.0	9.3	7.8
Head (X) (g)	-5.6	-6.6	-5.5
HIII, S – Hybrid III, Straight Spine			
HII – Hybrid II			
HIII, C – Hybrid III, Curved spine			

The results in Table 3 show very consistent data between all three ATD configurations. This is in contrast with the strong paper honeycomb results. These results suggest that the impact pulse, along with configuration of the ATD, will play a role in the results obtained.

As a check to ensure validity of the test results presented in Tables 2 and 3, photogrammetric measurements were taken to ensure that each ATD was positioned consistently for each repeated test in each configuration and that no anomalies existed to possibly skew the test data. Table 4 lists the maximum difference in position for the repeated tests for each test configuration, as measured by photogrammetry, along with its direction and location. In the case of the Hybrid II impacting the strong paper honeycomb, photogrammetric data was only able to be collected for one test, thus no comparisons can be made.

Table 4 – Positioning Consistency between repeated tests for a specific configuration

ATD, Spine, Honeycomb	Max diff.	Direction	Position
HIII, S,S	0.84"	X	Left Knee
HIII,S,W	0.42"	X	Head Top
HII,S,W	0.75"	Y	Head Top
HIII,C,S	0.92"	X	Left Arm
HIII,C,W	0.66"	Y	Left Knee
HIII, S, S – Hybrid III, Straight Spine, Strong Paper Honeycomb			
HIII, S, W – Hybrid III, Straight Spine, Weak Paper Honeycomb			
HII,S,W – Hybrid II, Straight Spine, Weak Paper Honeycomb			
HIII, C, S – Hybrid III, Curved Spine, Strong Paper Honeycomb			
HIII, C W – Hybrid III, Curved Spine, Weak Paper Honeycomb			

Table 4 shows that the maximum difference between retests in the same condition was less than 1 in. In three of the five tests, the difference was located in an appendage, while the other two showed the head leaning forward slightly. These results indicated that no anomalies were present when positioning the ATDs between repeated tests of the same test configuration.

Comparisons between the six test configurations were also completed to ensure positioning similarity between test configurations. This was to ensure validity of test results (especially the lumbar spine and pelvis accelerations for the strong paper honeycomb), between the different configurations tested. Table 5 shows these results.

Table 5 – Positioning Consistency between the different test configurations

ATD	Paper honeycomb	Max diff direction	Position
HIII, Straight to HIII curved	Strong	2.0"- X	Head Top
	Weak	1.9"-Z	Head Top
HIII, Curved to HII	Strong	3.6"-Z	Left Arm
	Weak	4.2"-Z	Left Arm
HIII, Straight to HII	Strong	3.3"-Z	Left Arm
	Weak	N/A	N/A
HIII – Hybrid III			
HII – Hybrid II			

The results do show, however, that the spine configuration affects how the upper body, and

especially the head, is positioned. The head acts as a cantilevered mass extending from a flexible neck connected to the spine. It is the furthest distance away from the spine, and thus, a small change in the spine configuration brings about the largest change in the head configuration. This important point explains the head positioning being the largest difference, when only the lumbar spine is changed in the Hybrid III ATD.

As previously mentioned, physical construction of the shoulder and arm were slightly different between the HII and the HIII, and constraints on the arms necessitated that the targets be placed at slightly different locations to correctly resolve angle and motion measurements. Therefore, it is expected to see the largest differences in position in the arms as shown in Table 5. The differences in the chest measurements (not shown in Table 5) averaged 1.56 in. lower in the Hybrid III with curved spine than the Hybrid III with the straight spine, which indicates that the curved spine reduces the total height of the ATD by approximately 1.56 in.

Finally, photogrammetric techniques were used in an example test to determine the amount of motion that occurred the ATD between the final positioning step (pre-test state) and immediately prior to impact (pre-impact state). The rationale was to check to see if the positioning would change between these two stages of the test, thus verifying that positioning procedures were robust. The pre-impact state of the ATD was the frame captured by the high speed cameras immediately before the ATD and platform contacted the paper honeycomb.

Distances between each target on the ATD and static targets on the platform were computed for both the positioned ATD and the pre-impact state of the ATD. The maximum difference in these two numbers for all three directions is reported in Table 6.

Table 6 – Position differences between pre-test and pre-impact (all units in inches)

	Vertical		Horizontal		Lateral	
	Avg.	*Max*	*Avg.*	*Max*	*Avg.*	*Max*
	0.38	0.74	0.22	0.77	0.04	0.05
Pos.	Top Head		Top Head		Top Head	

Table 6 shows that the maximum difference for all targets examined was approximately 0.77 in, which was measured in the horizontal axis at the top of the head. Table 6 also shows that the top of the head shows the most difference for all three directions, which is understood because, as previously postulated, the head rests the furthest away from the

seat platform, and therefore, a very small change in the position of the seat platform would be magnified in the head. However, all measurements were below 1 in., suggesting that the differences in the position of the ATD between the positioned state and the pre-impact state was small.

Occupant Injury Criteria

The seat pan acceleration time histories were compared to a series of injury curves originally developed by Eiband [17] in the late 1950s. Figure 10 shows an example of one of Eiband's curves, depicting injury thresholds for accelerations in the vertical direction. Table 7 shows the peak magnitude and duration of the pulse into the seat.
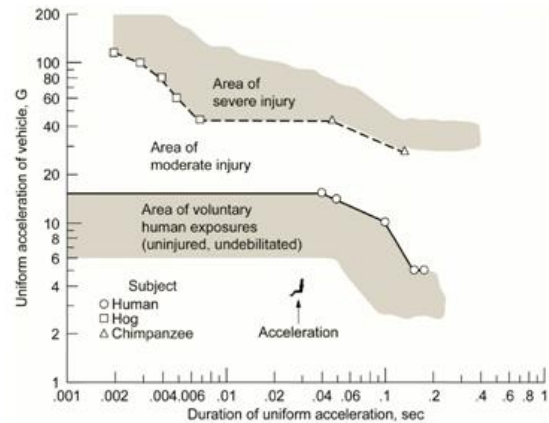

Figure 10. Eiband injury limit curve (reprinted from ref [17])

Table 7. Seat pan vertical peak accelerations and durations

Paper honeycomb	Peak accel. (g)	Pulse duration (s)	Eiband Regime
Strong	275	.004	Severe
Weak	33	.008	Moderate

Seat pan acceleration time history pulses in the forward, lateral, and vertical directions were input into the Brinkley model [18], which is used to evaluate injury risk in aircraft and spacecraft. The output result from the Brinkley model is an index, also known as a beta value, which into account responses from all three axes. The value of beta is given for three risk categories: low, medium and high. A beta value greater than or equal to one in a category pushes the risk probability to the next higher category until the value is less than one. Table 8 lists

the beta values for all occupants for both tests, with careful attention being paid to the values in italic.

Table 8. Brinkley Indices

Position	Beta Low	Beta Med.	Beta High
Strong	*1.19*	*1.00*	0.79
Weak	0.42	0.36	0.28

Application of the Eiband and Brinkley criterion to test data highlights the importance of the load magnitudes and durations an occupant could be exposed to in the event of an aircraft crash. If an occupant were exposed to a high acceleration magnitude, short duration pulse, similar to what was generated by strong paper honeycomb, the occupant would be at a high risk of injury. Likewise, if a low acceleration magnitude, high duration pulse was imparted into the occupant, he or she would experience a low risk of injury so long as the duration is not extended far along the abscissa axis on the Eiband graph.

The use of FAR 27.562 to determine injury risk is consistent with Eiband and Brinkley criterion results. As reported earlier, application of a high magnitude, short duration acceleration pulse produces lumbar load values greater than the allowable limit of 1,500 lbs than a low magnitude, long duration pulse. Thus, care must be taken to ensure that impact loads transmitted into an occupant are kept at a minimum in the event of an aircraft crash.

Finite Element Analyses of Drop Tests

Two different finite element model representations of the Hybrid III 50th Percentile ATD were evaluated in the vertical loading regime using the explicit, dynamic nonlinear finite element code LS-DYNA and compared with test data. One model was developed by First Technology Safety Systems (FTSS) [19] and the other by Livermore Software Technology Corporation (LSTC) [20]. Both models utilized the curved spine (automotive) configuration only. The FTSS Hybrid III model contained 100,822 nodes, 23,399 rigid elements, and 95,173 deformable elements. A picture of the model in the FTSS model in the test configuration is shown in Figure 11.
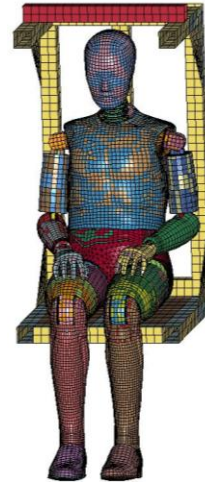

Figure 11 - FTSS model

One area of interest is the lumbar pelvic region on both models, due to the vertical nature of the loading. The FTSS lumbar pelvic region contains null shells for contact, pelvis skin represented by using a viscoelastic material model, and pelvis foam assigned a strain-rate dependent material model for low density foam. The pelvis skin was modeled using a constant solid stress element formulation, while the pelvis foam utilized a tetrahedron element formulation with one integration point through the element thickness. Contact was defined in the FTSS model using a global-based contact algorithm to account for all body parts contacting one another.

The LSTC Rigid-FE model of the Hybrid III ATD contains 7,444 nodes, 2,453 rigid elements and 1,842 deformable elements. A picture of the model in the test configuration is found in Figure 12. Unlike the FTSS model, the LSTC model only has the pelvis foam modeled, using hexagonal elements with one element through the thickness. The pelvis foam utilizes an isotropic material model for low density foams with a rate independent stress-strain curve defined.
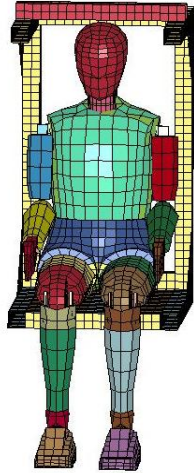
Figure 12 - LSTC model

Both models were setup such that impact conditions closely matched those of the test. Different acceleration time histories were applied on the seat platform bottom spread out over a cross-sectional area equal to the honeycomb dimensions from the tests. For each model, six cases were executed, where the acceleration time history input was based on the test condition (Hybrid II or Hybrid III, curved or straight lumbar spine, strong or weak paper honeycomb). Each input acceleration time history was filtered using a low pass 4-Pole Butterworth filter with a 1000 Hz cutoff frequency. In each case, the ATD models were positioned according to photogrammetry angular measurements, which included head, chest, and limbs.

The seat platform was assigned aluminum properties and a fully-integrated shell element formulation. Nodal constraints were applied over the platform box tubes to represent the bracket attachments simulating pure vertical motion along the drop tower rails. The boundary conditions in the seat model were important since both photogrammetry data and simulations showed that the input acceleration affected platform flexural response. Mass elements weighing 3 lbs each were added to the chair where the brackets were placed (two on each side of the platform), thus replicating the boundary conditions seen in testing. There were approximately 3,200 elements present in the platform model. A segment-based contact algorithm was implemented between the seat bottom and the pelvis and thigh of the ATD. The global coordinate system for all models corresponded to the test coordinate system.

Each model required detailed understanding of its features to obtain an acceptable correlation level between test and analysis. One of the first mechanisms studied was the effect of a preload into the ATD. The test results showed a preload of approximately 40 lbs of compression, measured prior to ATD and platform contact, in the lumbar load cell, indicating the ATD was compressing on the platform during the drop. A set of analyses was conducted using the FTSS model to assess the effect of varying the preload on the response of the ATD. This condition was simulated by varying the magnitude of gravity in the model to achieve an analogous preload into the pelvis. Models were run where the initial conditions varied and 0%, 20%, 30%, 35%, 50%, and 100% of a full gravity load were applied. The gravity load was applied as a preload condition prior to an acceleration time history pulse representing contact with the paper honeycomb. Conducting the analysis demonstrated that the response of the ATD was sensitive to the amount of preload applied to the pelvic region. Overall, peak head accelerations varied between 35 and 56 g's, peak chest accelerations varied between 35 and 61 g's, and peak pelvis accelerations varied between 55 and 110 g's.

The general trend observed was that as the gravitational scale factor increased, the peak acceleration magnitude decreased. This decrease is attributed to the pre-impact deformation of the pelvis mesh, which led to a decrease in the initial impulsive loads transferred into the pelvis during impact. Based on analytical results, 35% of full gravity load was chosen as the optimal value which should be applied to preload the dummy since the responses seen from the ATD best matched what occurred in the test series. Lumbar load readings in the model were taken from a discrete beam designed to measure lumbar forces in a local coordinate system. The lumbar load value of 47 lbs in the model best corresponded to the average load cell readings during free-fall in the test for a 35% gravity load. The positional changes of the ATD models between pre-release and pre-impact also best matched data obtained using high-speed videos with photogrammetry, and best represented the acceleration time histories obtained for the head, chest, and pelvic accelerations. Results showing the lumbar load cell preload values are found in Figure 13. Note that all preload values were read at Time=0 s, which occurs at the end of the preload phase, and right before the acceleration pulse is applied to the seat platform.
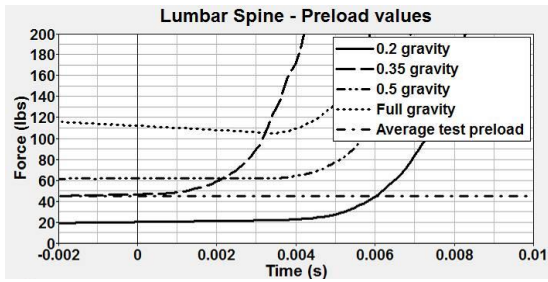
Figure 13 - Preload study results

To allow the pelvic regions in each ATD model to deform pre-impact, all chair nodes were fully constrained from motion for the first 100 ms of the simulation while the ATD became supported by the chair. The duration of the model was 150 ms for a strong paper honeycomb pulse input, and 200 ms for a weak paper honeycomb pulse input. The differences in model duration are present because the use of strong and weak paper honeycomb yield short and long pulse width durations respectively upon impact, respectively.

All models were run using 4 Linux-based processors using LS-DYNA version 971 R4.2.1 in double precision. Table 9 lists the run times for each case run using both models. Note that the LSTC models had a shorter run time than the FTSS model due to coarser detail in the LSTC model.

Table 9 - FTSS runtime vs. LSTC runtime

| ATD, Lumbar Spine config.	Paper honeycomb	FTSS Run Time	LSTC Run Time
HIII, Straight	Strong	8 h, 21 m, 19 s	22 m
	Weak	10 h, 56 m, 56 s	29 m
HII, Straight	Strong	8 h, 18 m, 49 s	22 m, 5 s
	Weak	9 h, 58 m, 32 s	29 m, 10 s
HIII, Curved	Strong	7 h, 30 m, 33 s	20 m, 25 s
	Weak	10 h, 55 m, 8 s	29 m, 39 s
HIII - Hybrid III, HII – Hybrid II			
h - hours, m - minutes, s – seconds			

Response data taken from the FTSS and LSTC models were compared with test data, as shown in Figures 14-17. Overall, the FTSS acceleration and lumbar load responses match the trends seen in the

test data regardless of the input acceleration type used for different ATD and lumbar spine configurations. The correlation level between the LSTC model results and test data in all impact cases is extremely low. One obvious trend seen in the model is that an initial spike appears immediately after impact in the lumbar, chest, and head regions. Secondary peaks not present in the test data occur in the acceleration time histories due to uneven initial distribution of impact loads acting upon the pelvis, and pelvis rotation occurring afterwards as a result of slouching in the occupant. The pelvic rotation affects how load is transferred into the ATD. Between the initial spike and when the second highest peak occurs (25 ms for strong paper honeycomb and 40 ms for weak paper honeycomb), the pelvis adjusts position where load is distributed on all pelvic foam segments contacting the seat. For purposes of comparing equal ATD and spinal configurations between physical and numerical entities, responses for a Hybrid III with a curved spine configuration are shown here. As shown in Figure 14, for both strong and weak paper honeycomb, the vertical head acceleration in the FTSS model matches the initial peak magnitude seen in the test responses before dropping, then rebounding due to increased load transfer into the head. A time lag between peak accelerations in the FTSS model and test data is present in all cases analyzed. The peak acceleration in the LSTC analysis is three times as high as that of the test using a strong paper honeycomb pulse, and twice as high using a weak paper honeycomb pulse. Generally, the LSTC results were indifferent to preload on the pelvis foam. More information on this issue can be found in the Discussion section of the paper.
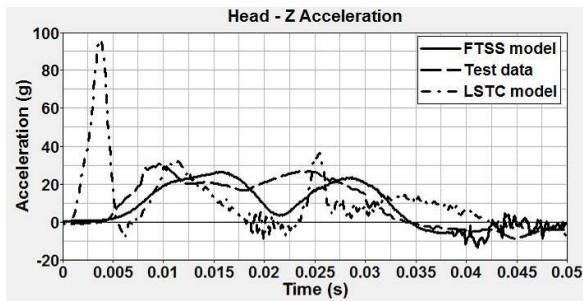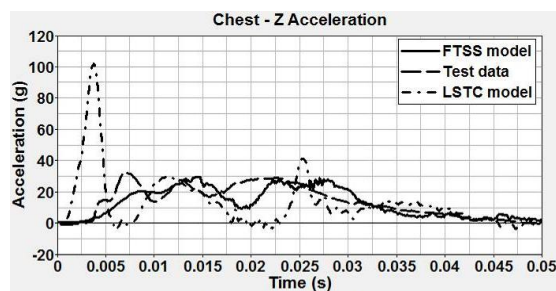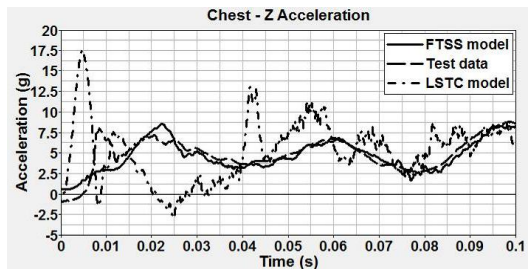
(a) Strong paper honeycomb
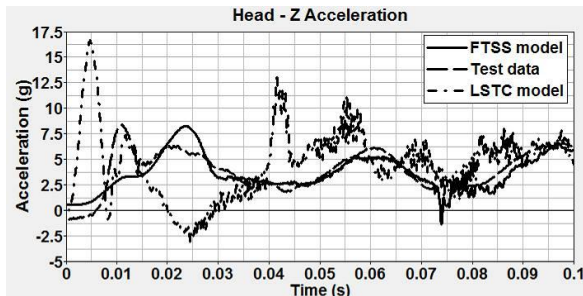
(b) Weak paper honeycomb

Figure 14 - Head acceleration responses for curved spine configuration in test and analysis

The vertical chest acceleration time histories in the FTSS and LSTC models exhibit similar trends as those seen in the head response, as shown in Figure 15. In the FTSS model, the acceleration magnitudes match with the test response before a slight drop in magnitude and rise before the curve drops again. This slight drop and rise comes from the load starting to pick up as it makes its way from the pelvis into the chest. When the weak paper honeycomb is used, the post-impact curve matches very well with test data. The LSTC model, however, shows an initial spike over prediction by about three times that seen in the chest using strong paper honeycomb, and about twice that seen using a weak paper honeycomb pulse. The secondary peak occurs, again, from redistribution of load transfer from pelvis foam segments into the ATD.
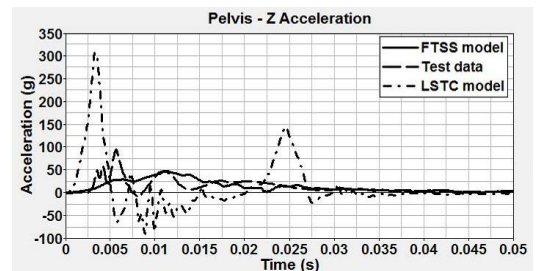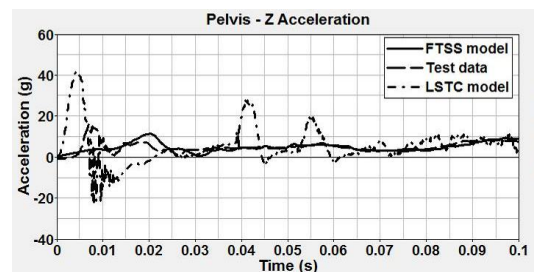

(a) Strong paper honeycomb

(b) Weak paper honeycomb

Figure 15 - Chest acceleration responses test/analysis comparison for curved spine configuration

The pelvis and lumbar spine responses, shown in Figures 16 and 17, in the FTSS model agree very well with test data, particularly the post-impact trends and magnitudes. A slight under prediction in vertical pelvis acceleration occurs when strong paper honeycomb is used. In the LSTC model, the vertical accelerations are over predicted by three times the values seen in the test data. The lumbar loads are over predicted by three times the test values using a strong paper honeycomb input, while the loads are over predicted by twice those seen in the test data using a weak paper honeycomb pulse. The two spikes present in the time histories for the pelvis and lumbar spine are attributed to reorientation of pelvis segments with respect to the seat bottom, due to rotation of the pelvis throughout the simulation. All analytical curves from the LSTC model were filtered using SAE CFC 600.
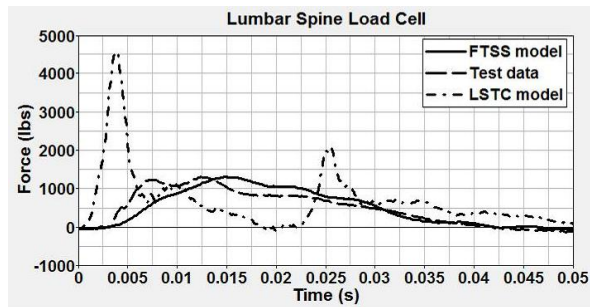

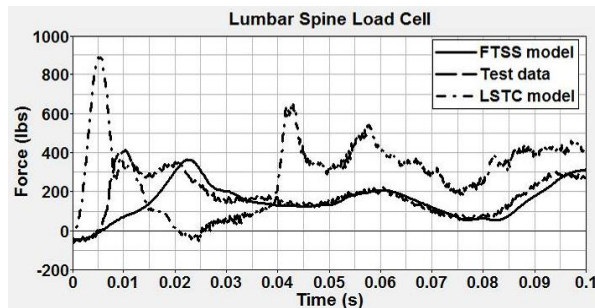(a) Strong paper honeycomb

(b) Weak paper honeycomb

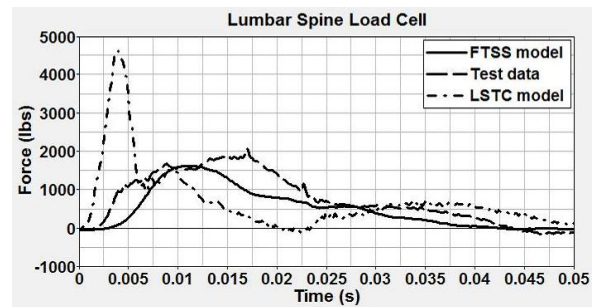Figure 16 - Pelvis acceleration response test/analysis comparison for curved spine configuration
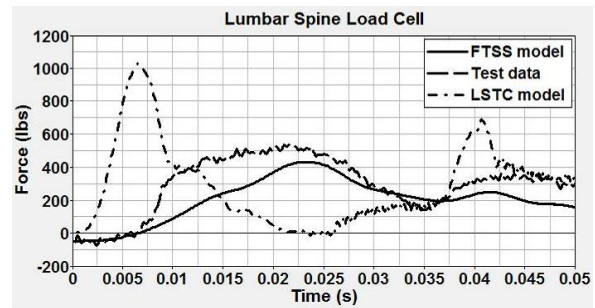
(a) Strong paper honeycomb

(b) Weak paper honeycomb

Figure 17 - Lumbar load response test/analysis comparison for curved spine configuration

(a) Strong paper honeycomb

(b) Weak paper honeycomb

Figure 18 - Comparison of lumbar load between Hybrid III ATD with straight spine and model

Correlation between FTSS model and test data is very good when comparing the Hybrid III model to a physical Hybrid III with a curved spine configuration. However, if the Hybrid III model response is compared with the response of a physical Hybrid III ATD with a straight spine, the discrepancy between test and analysis becomes more prevalent. Figure 18 shows the lumbar load readings taken from the FTSS and LSTC models. The pulse duration in the FTSS model is smaller than in the test using strong paper honeycomb, while the pulse duration is longer than in the test using weak paper honeycomb. The LSTC model still does not match test data, over predicting the test lumbar load by a factor of 2.5 for strong paper honeycomb, and a factor of 2 for weak paper honeycomb. The spike at 40 ms in the LSTC response using weak paper honeycomb comes from an increase in load transfer due to reorientation of pelvis foam segments. While, for aerospace applications, it is convenient to represent a sitting occupant using a straight spine in an ATD, there is no direct comparison that can be made since the lumbar spine configuration differs physically and numerically, which can affect the vertical load path into the ATD.

One aspect that was examined for improvement in the analysis using the FTSS Hybrid III was the time lag that existed between peak accelerations and lumbar loads. As a result, a case was run which examined the pelvis foam stiffness on the overall response of the ATD. An arbitrary scale factor of 10 was applied on the ordinate values of the stress-strain input curves for pelvis foam. Using the same model setup as previously described, the FTSS model with modified pelvic foam was re-run. In general, stiffening the pelvis foam eliminates the time lag. The vertical head acceleration peak values are slightly under predicted. However, the trends exhibited in the test during impact and post-impact are well predicted by the model using both strong paper honeycomb and weak paper honeycomb input pulses, as shown in Figure 19.
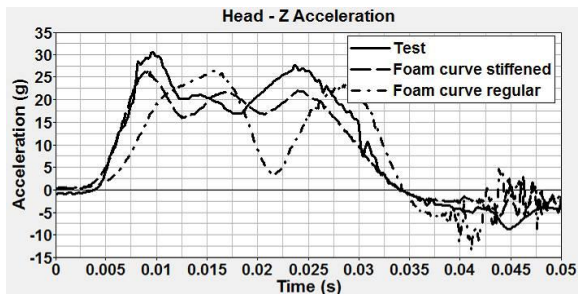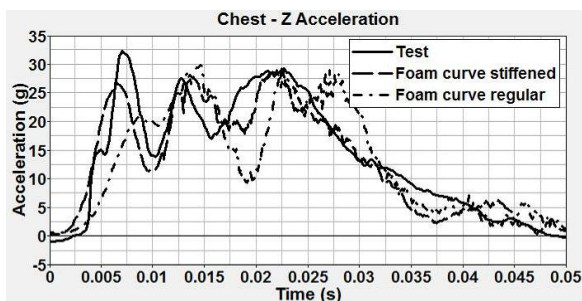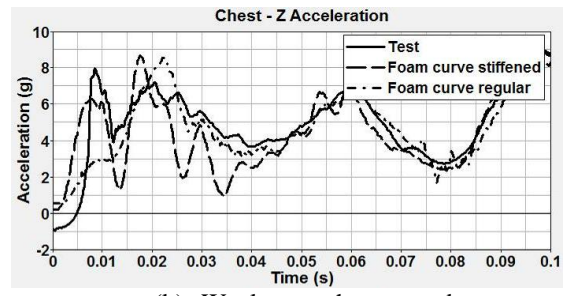
(a) Strong paper honeycomb
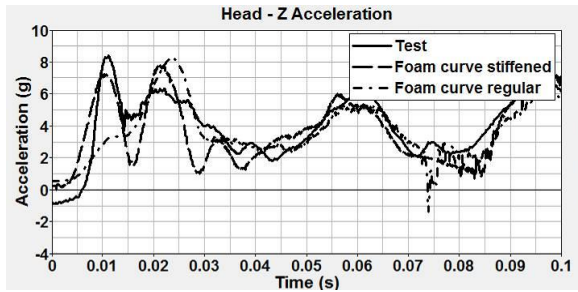
(b) Weak paper honeycomb

Figure 19 - Head acceleration responses for curved spine configuration in pelvis foam stiffness study (FTSS Model)

The double peaks seen in the chest acceleration time history are captured when the pelvis foam is stiffened and a strong paper honeycomb pulse is applied to the seat bottom, as shown in Figure 20(a). While the magnitude of the acceleration peak is slightly under predicted, the post-impact response of the ATD closely follows the test data. More peaks are present when a weak paper honeycomb pulse is applied into the occupant model, possibly due to elastic rebound of the pelvis foam leading to softer loads being transferred into the occupant, shown in Figure 20(b).
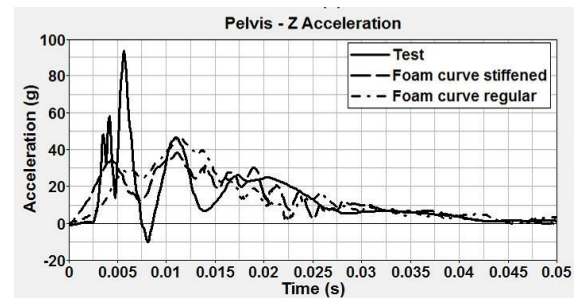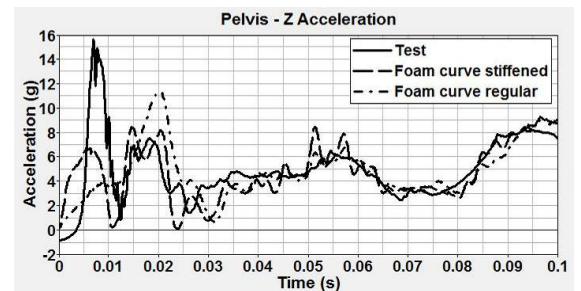

(a) Strong paper honeycomb

(b) Weak paper honeycomb

Figure 20 - Chest acceleration responses test/analysis comparison for curved spine configuration in pelvis foam stiffness study

The occurrence of the peaks in the acceleration and lumbar load time histories match well with the test data when both pulse shapes are imparted into the seat, as shown in Figures 21 and 22, respectively. The initial peak accelerations and lumbar loads under predict those of the test, due to greater strain energy required to deform the mesh to levels seen before the foam was stiffened. This explanation also accounts for the slight over prediction in peak lumbar load when the strong paper honeycomb pulse shape was driven into the occupant. Nonetheless, time history trends were better represented when the pelvis foam stress-strain curves were stiffened.
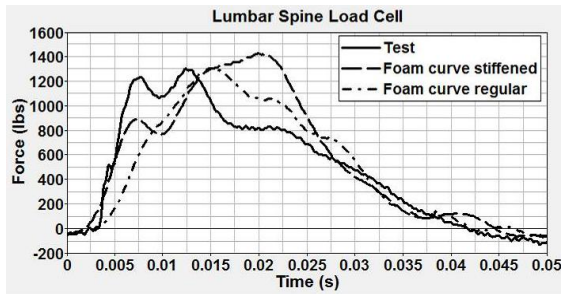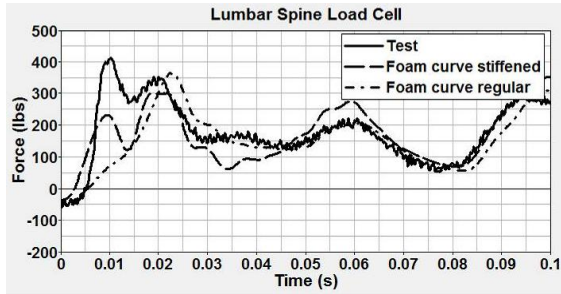

(a) Strong paper honeycomb

(b) Weak paper honeycomb

Figure 21 - Pelvis acceleration response test/analysis comparison for curved spine configuration in pelvis foam stiffness study

(a) Strong paper honeycomb


(b) Weak paper honeycomb

Figure 22 - Lumbar load response test/analysis comparison for curved spine configuration in pelvis foam study

Discussion

The LSTC Hybrid III model predictions show extremely poor correlation with the test results. One reason why this discrepancy could exist is attributed to the lack of detail in the pelvic region. Figure 23 shows a cross-section of both the FTSS and LSTC models. The pelvis in the LSTC model is overly stiff, characterized by only 328 elements and one hexagonal element through the thickness, versus 23,280 elements for the FTSS pelvis model and up to 9 tetrahedral elements through the thickness. During the preload phase of the simulation, it was noticed that little to no strain energy goes into deforming the LSTC pelvis mesh.
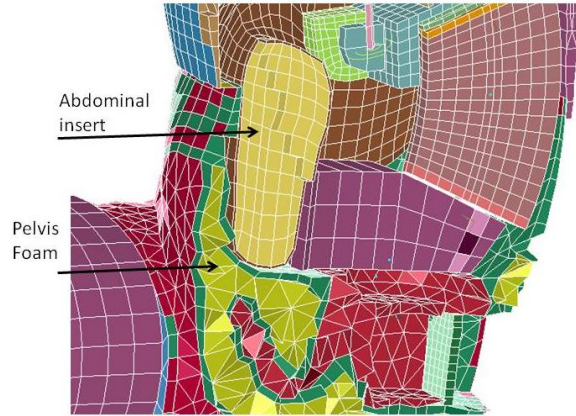
(a) FTSS pelvis cross-section
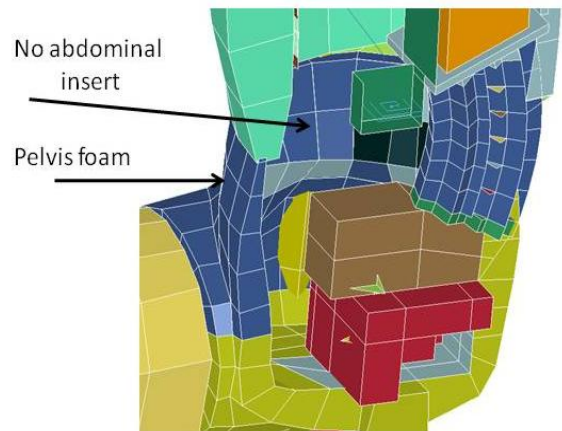
(b) LSTC pelvis cross-section

Figure 23 - Cross-sectional views of ATD models

In addition, less deformation of the LSTC pelvis foam can be attributed to a stiffer stress-strain curve in comparison to the FTSS stress-strain curves. The LSTC stress-strain material property curve is defined such that compaction occurs at 40 percent strain versus compaction at 60 percent strain for the 10 s^{-1} and 100 s^{-1} strain rates seen in the FTSS pelvis foam model, as shown in Figure 24.
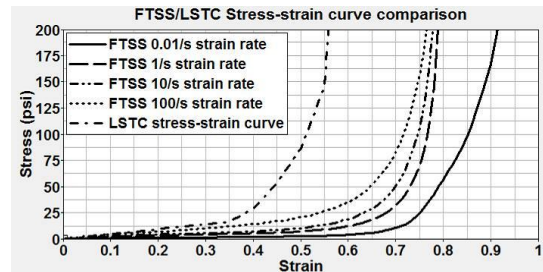

Figure 24 - Pelvis foam stress-strain curves

Rigid thighs in the LSTC model are another artifact of the model which likely contributes to excessive load transfer into the occupant. If the thighs were allowed to deform, the load magnitude transferred into the ATD model could be reduced, since a joint connection between the pelvis and the thigh facilitates vertical load transfer. In addition, the thighs only contain one element through the thickness. Reduced load transfer could also be achieved by increasing the number of elements through the thickness of the thigh.

The lack of compressibility in the LSTC pelvis model is complemented by an absence of an abdominal insert, as shown in Figure 23(b). The absence of an abdomen leaves the spinal column to transfer all of the impact forces into the upper portion of the ATD, since the abdomen naturally acts as a buffer to the occupant during load transfer. Likewise, contact is not defined in the model between the chest and the pelvis, leaving a missed crucial path for load transfer. Both of these missing features of the model attribute themselves to unrealistic movement of the ATD, such as slouching and excessive movement of the torso skin, as shown in Figure 25. In addition, the excessive forward motion of the torso alters the pre-impact position of the ATD and, thus, affects the overall impact response.
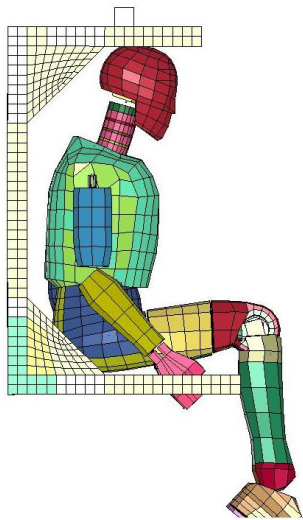
(a) LSTC dummy slouching forward
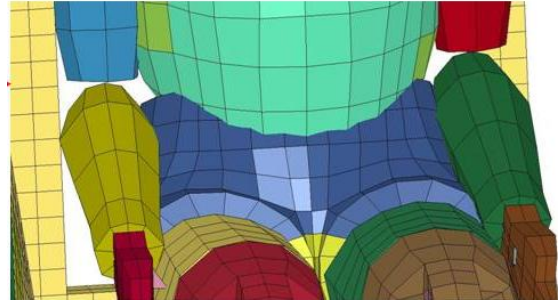
(b) Close-up of torso interaction with pelvis

Figure 25 - No contact definition between thorax and pelvis

Another problem which could have affected the ATD vertical response is the lack of flexibility within the positioning interface. Unlike the FTSS model, the pelvis and the torso in the LSTC model could not be positioned as separate entities. Thus, the pelvis had to be positioned at an angle from the thighs in order to match the model position with photogrammetry measurements. A case was run with the FTSS model where the angle between the pelvis and the thigh was zero and compared with a non-zero angle. Aligning the pelvis with the thighs led to an improvement in correlation by as much as 6.5% among peak accelerations and 3% for lumbar load, and improved time lag by 12.5% for accelerations and 6% for the lumbar load pulse.

Lastly, for the LSTC Model, the lumbar spine is placed in the model such that it penetrates through the pelvis foam. In turn, contact forces from the pelvis or torso skin would not transfer onto the lumbar spine and resist any bending moment coming from the spine. While the LSTC ATD was developed mainly for automotive applications, the present condition of the model does not make it suitable for vertical occupant response representation. Many important features are missing which are crucial to accurately transferring load from the lumbar region up into the occupant.

Conclusion

A series of vertical impact tests were conducted which compared the responses of the Hybrid II and Hybrid III Anthropomorphic Test Devices based on different spinal configurations and two different input acceleration pulse shapes imparted into the dummy. Based on seat pan accelerations from the test, applying a high magnitude, short duration acceleration pulse into an occupant provides a higher risk for injury in the event of a crash than if a low magnitude, long duration acceleration pulse was

applied. The test data acquired was then used to compare and evaluate the performance of two vendor Hybrid III automotive finite element models by FTSS and LSTC under vertical impact. The FTSS model achieved better correlation than the LSTC model with test data given that the FTSS ATD is more detailed overall. A preload was applied to the pelvis foam, allowing it to deform, and the stress-strain curves for pelvis foam were stiffened. The LSTC model lacks detail, especially in the pelvis region, that does not allow efficient load transfer in the vertical direction. While neither model is best suited for prediction of occupant injury, modifications in the lumbar region of the occupant could be made to both ATD models which would improve their fidelity in the vertical loading regime.

References

[1] Nahum, A.M and J.W. Melvin, ed. "Accidental Injury: Biomechanics and Prevention 2nd ed." Springer-Verlag, New York. 2002.

[2] U.S. Department of Transportation. "Federal Motor Vehicle Safety Part 571, Standard 208 – Occupant Crash Protection" www.fmcsa.dot.gov. Accessed 11-12-10.

[3] Code of Federal Regulations, Federal Aviation Regulations for Aviation Maintenance Technicians FAR AMT, Part 27 Airworthiness Standard: Normal Category Rotorcraft, 27.562 Emergency Landing Dynamics.

[4] Gowdy, V. et al. "A Lumbar Spine Modification to the Hybrid III ATD for Aircraft Seat Tests". SAE 1999-01-1609. 1999.

[5] Kellas, S., Jackson, K., and Littell, J., "Full Scale Crash Test of a MD 500 Helicopter with Deployable Energy Absorbers," Proceedings of the 66th AHS Annual Forum, Phoenix, AZ, May 11-13, 2010.

[6] Littell, J. "Full-Scale Crash Test of an MD-500 Helicopter." Proceedings of the 67th AHS Forum, Virginia Beach, VA, May 3-5, 2011.

[7] Jackson, K.E. et al. "Occupant Responses in a Full Scale Crash Test of a Sikorsky ACAP Helicopter." NASA TM 2002-211733. 2002.

[8] Jones, L.E. and H.D. Carden. "Overview of Structural Behavior and Occupant Responses from a Crash Test of a Composite Airplane." NASA TM-111954. 1995.

[9] Fasanella, E.L. and K.E. Jackson. "Impact Testing and Simulation of a Crashworthy composite Fuselage Section with Energy-Absorbing Seats and Dummies". Proceedings of the 58th AHS Annual Forum, Montreal, Canada, June 11-13, 2002.

[10] Rapaport M., et. al. "Establishing a Spinal Injury Criterion for Miltary Seats" Naval Air Warfare Center, A831644. 1997.

[11] Hu, D.Y. et al. "Full-Scale vertical Drop Test and Numerical Simulation of a Crashworthy Helicopter Seat/Occupant System." International Journal of Crashworthiness, Vol. 14, No 6, pp 565-583. 2009.

[12] Salzar, R.S. et al. "Ejection Injury to the Spine in Small Aviators: Sled Tests of Manikins vs. Post Mortem Specimens." Aviation, Space, and Environmental Medicine, Vol 80, No. 7. Pg 621-629. 2009.

[13] Buhrman, J.R. "Vertical Impact Tests of Humans and Anthropomorphic Manikins" AL-TR-1991-0129. 1991.

[14] Perry, C. et al. "Evaluation of Proposed Seat Cushions to Vertical Impact". Proceedings of the 38th Annual SAFE Symposium, 2000.

[15] Lawrence, C. et al. "The Use of a Vehicle Acceleration Exposure Limit Model and a Finite Element Crash Test Dummy Model to Evaluate the Risk of Injuries During Orion Crew Module Landings" NASA TM 2008-215198. 2008.

[16] Society of Automotive Engineers. "Surface Vehicle Recommended Practice: Instrumentation for Impact Test-Part 1-Electronic Instrumentation". SAE J211-1, July 2007.

[17]   Eiband, A.M.   "Human Tolerance to Rapidly Applied Accelerations: A summary of the Literature," NASA Memorandum 5-19-59E. 1959.

[18]   Brinkley, J.W., Specker, L.J., and Mosher, S.E., "Development of Acceleration Exposure Limits for Advanced Escape Systems."   NATO AGARD Proceedings, AGARD-CP-472, February 1990.

[19] First Technology Safety Systems. "FTSS LS-DYNA Model of the Hybrid III 50th Percentile Male Dummy User Manual," Version 7.0, December 2008.

[20] Anon, "LS-DYNA Keyword User's Manual," Version 971, Livermore Software Technology Company, Livermore, CA, August 2006.